Computational Materials Science 133 (2017) 122–129

Contents lists available at ScienceDirect

Computational Materials Science

journal homepage: www.elsevier.com/locate/commatsci

Two-dimensional honeycomb (A7) and zigzag sheet (ZS) type nitrogen monolayers. A first principles study of structural, electronic, spectral, and mechanical properties

Sergey V. Bondarchuk [a,*], Boris F. Minaev [a,b]

[a] Department of Chemistry and Nanomaterials Science, Bogdan Khmelnitsky Cherkasy National University, blvd. Shevchenko 81, 18031 Cherkasy, Ukraine
[b] Division of Theoretical Chemistry and Biology, School of Biotechnology, KTH Royal Institute of Technology, 10691 Stockholm, Sweden

ARTICLE INFO

Article history:
Received 15 November 2016
Accepted 3 March 2017

Keywords:
Nitrogen allotropes
2D materials
Single-bonded nitrogen
DFT
High-energy density materials

ABSTRACT

Two single-bonded 2D nitrogen allotropes of the honeycomb (**A7**) and zigzag sheet (**ZS**) topology have been calculated using density functional theory (DFT). The optical (vibrational, absorption, nuclear magnetic resonance), thermodynamic and elastic properties of the **A7** and **ZS** sheets have been calculated for the first time. The band structure calculation have revealed a semiconducting nature of the **ZS** sheet with a direct gap of 1.246 eV, while the **A7** monolayer behaves as an insulator with an indirect gap of 3.842 eV. Phonon dispersion calculations have justified these structures as vibrationally stable 2D materials. The IR spectroscopy completely failed in the characterization of the studied materials, while the Raman spectroscopy can be effectively applied for the experimental spectral identification. The absorption spectra demonstrate complete opacity of the **A7** and **ZS** monolayers to the UV irradiation only above ca. 9 and 6 eV, respectively. Thus, the studied materials are expected to be transparent to the visible light. The electron arrangement of the nitrogen nuclei in the studied polynitrogen sheets is denser compared to the N_2 molecule which follows from the calculation of the values of magnetic shielding tensors. The elastic constants reveal a robust mechanical stability of the studied 2D nitrogen allotropes. The Young moduli values are only twice as lower than that of the graphene molecule.

1. Introduction

The discovery of graphene has opened up new horizons in the field of materials science [1]. This was the start of a new era for two-dimensional (2D) structures, which still attract a sustainable remarkable attention of both theorists and experimentalists [2]. In the family of 2D materials, nitrogen became an outcast for a long time. This is because of a very strong N≡N bond (954 kJ mol^{-1}), which forms one of the most stable molecules known. Thus, only in 2014 the first report on the epitaxial 2D nitrogen atomic sheet in GaAs was published [3]. However, the topology of this sheet has not been determined. To our knowledge, only one very recent paper has been published on the theoretical study of 2D nitrogen honeycomb structure [4]. In the case of "zigzag" sheet, there are no direct calculations, except the modeling of layered polymeric "zigzag" structure [5].

Meanwhile, the modification of various 1D and 2D materials by means of the nitrogen atoms insertion has been intensively studied. The aim of such modification is a searching for new potential semiconductors possessing direct band gaps of about 1.4 eV. Thus, boron-nitrogen [6] boron-nitrogen-carbon monolayers [7], nitrogen-carbon holey sheets [8] and nitrogen-doped graphene nanoribbons [9–12], have been reported. Apart of the planar structures, a particular attention has been paid to studying the nitrogen-doped boron [13] and carbon [14–17] nanotubes. The latter demonstrate an effective electrocatalytic activity for oxygen reduction.

At near-ambient conditions, nitrogen exists exclusively in the molecular form. Thus, it becomes obvious that single-bonded nitrogen species should have huge energy content and represent the so-called high energy density materials (HEDM). Searching for potential HEDM composed only of nitrogen atoms was performed using different computational techniques [18–32]. A number of different neutral and ionic species was subsequently found. Among the vibrationally stable structures one can find the N_3^- [18], N_4 [19,20], N_5^- [21–23], N_5^+ [22,24], N_6 [25–29], N_8 [29], N_{10} [30] and N_{60} [31,32] species. However, among the aforementioned nitrogen forms, only three ionic structures were observed experimentally [18]. The azide anion (N_3^-) has a moderate stability, while

* Corresponding author.
E-mail address: bondchem@cdu.edu.ua (S.V. Bondarchuk).

http://dx.doi.org/10.1016/j.commatsci.2017.03.007
0927-0256/

the pentanitrogen cation (N_5^+) is metastable and can exist only with large counter anions. Finally, the pentanitrogen anion (N_5^-) has been detected both in the gas phase [21,22] and very recently in the crystalline form [23].

Another very interesting nitrogen allotrope, single-bonded cubic gauche structure (cg-N), was first predicted theoretically in far 1985 and then developed in 1992 by McMahan et al. [33,34]. Much later, in 2004, Eremets et al. obtained the cg-N allotrope using laser-heated diamond anvil cell experiments above 2000 K and 110 GPa [35]. At ambient temperature cg-N is metastable at pressures above 42 GPa and has unique properties including an energy density of about 27.89 kJ g^{-1} [35–37]. Although the all-nitrogen species has restricted functionality to date, the other HEDM with a high nitrogen content (nitrogen-rich) compounds demonstrate enhanced explosive features and environmental safety [18,38–45]. These compounds are characterized by high heats of formation, high explosive power, high ballistic properties, and high flame temperatures [18,40]. From ecological point of view, this is an environmental friendly type of HEDM, because the main gaseous explosive product is molecular nitrogen [18,39,46].

2. Computational details

The calculations presented in this paper have been performed using Cambridge Serial Total Energy Package (CASTEP) module [47] implemented in Materials Studio 7.0 program suite [48]. Exchange and correlation interactions were described using the generalized gradient approximation (GGA) approach with the functional parameterized by Perdew-Burke-Ernzerhof (PBE) [49]. To describe the electron-core interactions, a norm-conserving pseudopotential in reciprocal space has been used entirely. For calculations, the electronic wave functions have been expanded in a plane wave basis set with an energy cutoff of 1000 eV (73 Ry). The Monkhorst-Pack k-point sampling scheme with a $6 \times 6 \times 2$ k-point grid for supercell has been specified during all the calculations, except phonon dispersion. A denser k-point mesh ($8 \times 8 \times 4$) has been applied in the latter case to avoid a known problem with artifact out-of-plane acoustic branch (ZA branch) evolution around the Γ-point. Thus, an insufficient mesh size causes the negative values of the corresponding ZA branch. The SCF tolerance was set to 1×10^{-6} eV per atom.

The modeling of nitrogen sheets has been performed using the supercell approach. To avoid unphysical interactions between the neighboring layers, a 15 angstrom vacuum slab has been subsequently added. This has led to the formation of cells of the *P*-3*m*1 (**A7**) and *Pmm*2 (**ZS**) space group. Thereafter, the complete cell relaxation has been allowed. To take into account the long-range electron correlations, the Tkatchenko-Scheffler scheme has been applied entirely during the calculation [50]. This presents an accurate nonempirical method to obtain molecular C_6 coefficients from the ground-state electron density and reference values for the free atoms operating with polarizability and volume [50]; this approach has been proven to give reliable results [51]. Thus, the C_6 coefficients are calculated as the following:

$$C_{6AA}^{\text{eff}} = \frac{\eta_A^{\text{eff}}}{\eta_A^{\text{free}}} \left(\frac{\kappa_A^{\text{free}}}{\kappa_A^{\text{eff}}}\right)^2 \left(\frac{V_A^{\text{eff}}}{V_A^{\text{free}}}\right)^2 C_{6AA}^{\text{free}}, \quad (1)$$

where η is an effective frequency, V is the atomic volume, κ is the proportionality constant between volume and polarizability for the free atom and atom in a molecule. Superscripts "free" and "eff" stand for the isolated atom and the atom in a molecule, respectively. The performance of this scheme, when coupled with the PBE functional, is significantly better than for highly empirical C_6R^{-6} approaches [50].

The excess of energy (E_{excess}) has been calculated according to the following equation:

$$E_{\text{excess}} = E_{\text{sheet}} - nE_{N_2}, \quad (2)$$

where n is a stoichiometric coefficient, which equals to 2 and 1 for the **ZS** and **A7** sheets, respectively; E_{N_2} and E_{sheet} are the total energies (PBE-TS) of the nitrogen molecule and the corresponding sheet.

3. Results and discussion

3.1. Structural features and energy densities

The symmetry unique structural parameters of the studied polinitrogen sheets are illustrated in Fig. 1 and the packing of the layers is presented in Fig. S1 in the Supporting Information. It is clearly seen in Fig. 1 that the studied sheets are singly bonded. The N—N bond lengths are equal to 1.53 Å which are slightly longer than that of the cg-N (1.4 Å) [33,34]. On the other hand, the calculated N—N bond lengths are much closer to that of the black phosphorus-like (BP) nitrogen allotrope (1.53–1.54 Å); these values were obtained in terms of local density approximation [33,34,52].

Among the eleven proposed nitrogen forms the cg-N allotrope was found to be the most favorable (0.97 eV/atom) [34]. We have also performed the calculations of a relative excess of energy compared to α-N_2 using Eq. (2). The results revealed that the **A7** and **ZS** sheets have the E_{excess} values equal to 1.68 and 1.83 eV/atom, respectively. The first value, however, is closer to a previously obtained for **BP** phase (1.55 eV/atom), while the second value is the same as for the **A7** species (1.83 eV/atom) [34].

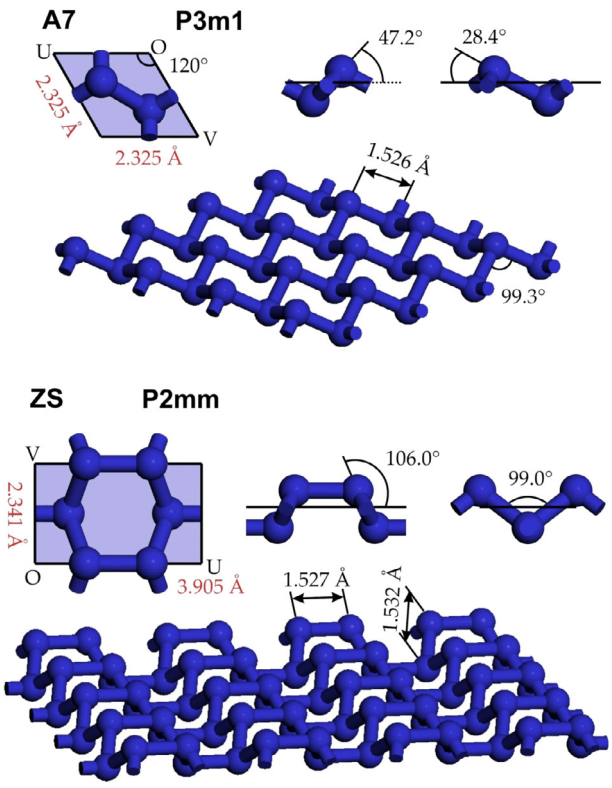

Fig. 1. The optimized structural parameters together with the three projections of the unit cell for the polynitrogen sheets studied.

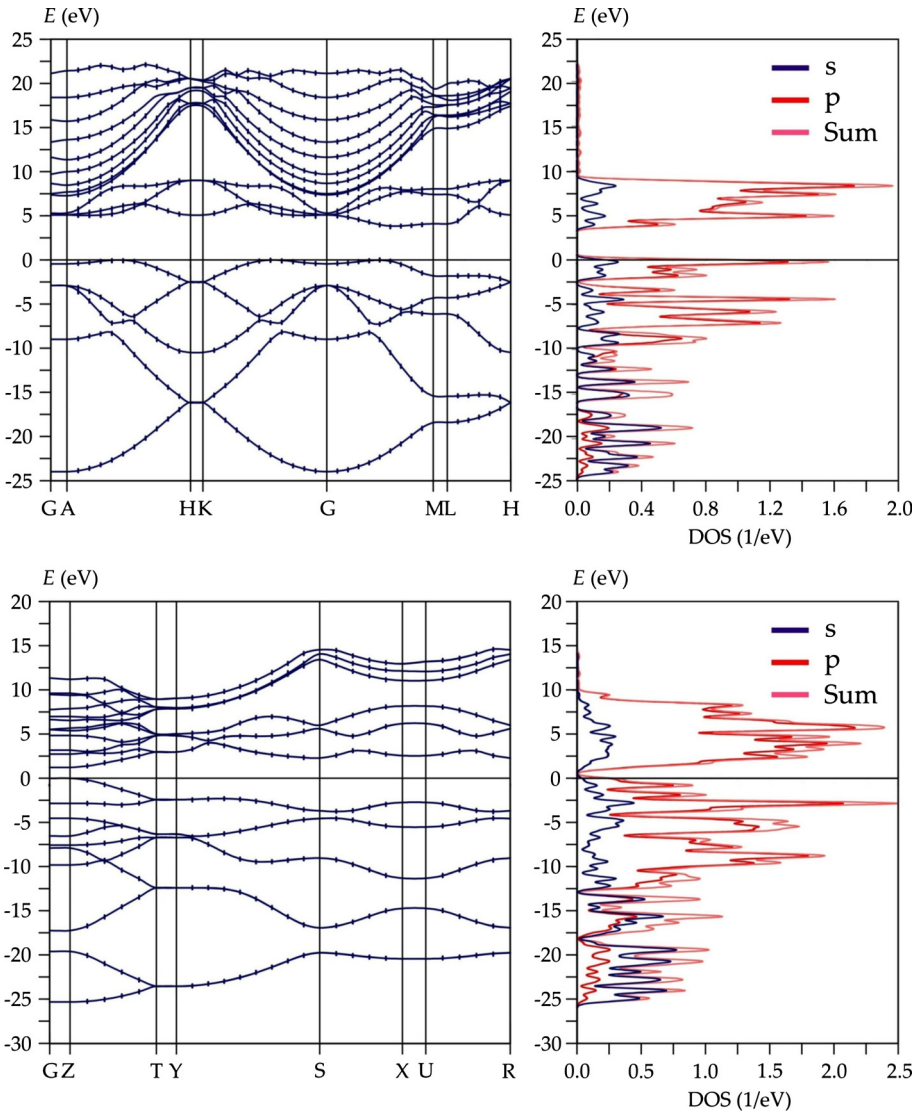

Fig. 2. The calculated band structure and partial density of states for the **A7** (top) and **ZS** (bottom) sheets studied.

3.2. Electronic structure and phase stability

The calculated band structure and partial density of states are illustrated in Fig. 2. The positions of valence band maximum (VBM) and conducting band minimum (CBM) indicate an indirect band gap (3.842 eV) in the case of the **A7** sheet and a direct band gap (1.246 eV) in the case of the **ZS** sheet (Fig. 2). The latter value is close to ~1.4 eV which is desirable for 2D materials being potential candidates for next-generation optoelectronics (in solar converting efficiency) [52]. It is remarkable that the VBM occurs not at the Γ-point in the case of **A7** monolayer. It is known that for the bulk materials this often be the case, whereas for the monolayered materials the VBM occurs at a *k*-point, rather than the Γ-point [7]. In contrast, in the case of **ZS** monolayer the VBM occurs at the Γ-point (Fig. 2). This situation is similar to the black [53] and blue [54] phosphorus monolayers.

In order to estimate phase stability of the **A7** and **ZS** monolayers we have performed phonon dispersion calculations. The phonon dispersion spectra of the studied nitrogen sheets along the high-symmetry lines in the Brillouin zone are shown in Fig. 3. The primitive cells of the **A7** and **ZS** monolayers contain two and four atoms, respectively; this gives rise to total 6 and 12 phonon branches. As one can see in Fig. 3, there are three acoustic modes: longitudinal (LA), transverse (TA) and flexural (ZA). Within the region of small *k*-point values, all the acoustic branches maintain the linear dispersion in the case of both the **A7** and **ZS** sheets (Fig. 3). Optical phonon branches of the **A7** sheet include one doubly degenerated and one nondegenerate mode. In the case of the **ZS** monolayer all the nine modes are nondegenerate.

It is clearly seen in Fig. 3 that all phonon modes in the **A7** and **ZS** monolayers have positive frequencies indicating these structures to be vibrationally stable. We should stress, however, that the phonon spectra have been calculated using the finite displacement method with an ultrasoft pseudopotential being a more effective in this case [55]. It is worthwhile noting that the phonon spectra calculation using a less expensive linear response approach along with a norm-conserving pseudopotential cause the negative values of the flexural ZA branch at the Γ-point.

3.3. Spectral pattern

The calculated IR and Raman spectra of the studied polynitrogen sheets are listed in Table 1. The spectrum of the **A7** sheet consists of two degenerated modes of the e_g symmetry and one mode

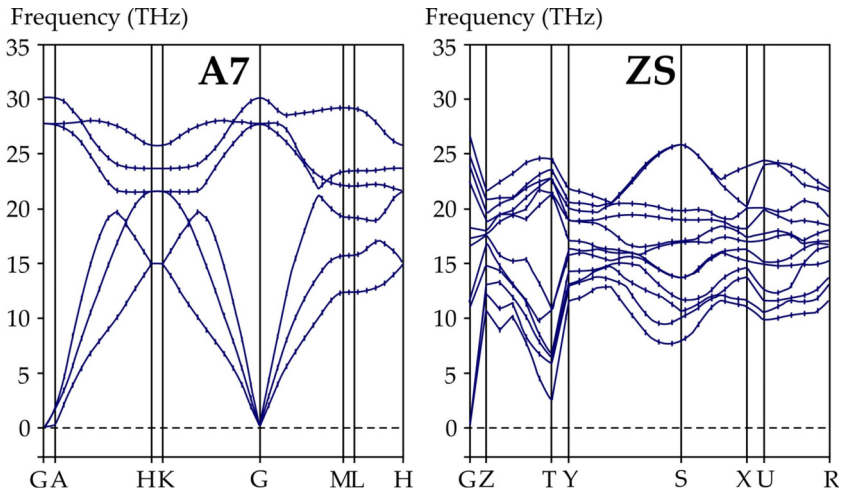

Fig. 3. The calculated phonon dispersion for the polynitrogen sheets studied.

Table 1
The calculated IR and Raman spectra of the polynitrogen sheets studied.

Mode	Symmetry	ν (cm^{-1})	IR (km mol^{-1})	Raman (A^4)
A7				
1	e_g	943.8	0.0	154.3
2	e_g	943.8	0.0	151.8
3	a_{1g}	1071.8	0.0	447.4
ZS				
1	b_2	321.3	160.1	0.4
2	a_2	408.9	0.0	0.0
3	b_1	683.5	0.0	5.7
4	a_1	758.8	0.0	24661.6
5	a_1	784.6	0.0	326.4
6	b_2	823.1	0.1	5.9
7	a_2	896.1	0.0	6275.9
8	a_1	911.8	0.0	1698.7
9	b_2	929.3	0.1	0.0

of the a_{1g} symmetry (Table 1). All the modes are Raman active with high intensities, but the IR transitions are forbidden by symmetry. The forms of vibrations are illustrated in Fig. S2 in the Supporting Information. In contrast, all the modes in the IR spectrum of the **ZS** monolayer are non-degenerate (Table 1). Though, three modes in the vibrational spectrum are IR active, only the first out-of-plane vibration of the b_2 symmetry has a noticeable intensity. This fundamental transition is not accessible for standard IR spectrometers. Meanwhile, the Raman spectrum is much more informative (Table 1). Only two vibrations have zero intensity, while four of the rest modes demonstrate very high Raman activity, especially, the mode of the a_1 symmetry at 758.8 cm^{-1} (24661.6 A^4). This is a type of the surface enhanced Raman band.

We have also calculated the optical properties of the **A7** and **ZS** nitrogen monolayers. The calculations are based on the estimation of the complex dielectric function $\varepsilon(\omega) = \varepsilon_1(\omega) + i\varepsilon_2(\omega)$. The imaginary part of this function includes momentum matrix elements, which allow to describe the electronic transitions between valence and conducting bands in a solid (Eq. (3)).

$$\varepsilon_2(\omega) = \frac{1}{4\pi\varepsilon_0}\left(\frac{2\pi e}{m\omega}\right)^2 \sum_{\mathbf{k},c,v} |\langle \psi^c_{\mathbf{k}} | ep | \psi^v_{\mathbf{k}} \rangle|^2 \delta(E^c_{\mathbf{k}} - E^v_{\mathbf{k}} - \hbar\omega) \quad (3)$$

Herein, subscripts c and v indicate conducting and valence band states, respectively.

The real part of the function is usually obtained from the imaginary part by means of the Kramer-Kronig transform (Eq. (4)) [56]:

$$\varepsilon_1(\omega) = 1 + \left(\frac{2}{\pi}\right) \int_0^\infty \mathrm{d}\omega' \frac{\omega'^2 \varepsilon_2(\omega')^2}{\omega'^2 - \omega^2} \quad (4)$$

A number of different optical properties—absorption coefficient, reflectivity, refractive index, conductivity, and loss function—can be obtained as derivatives of the dielectric function.

Thus, the absorption coefficient (α) can be derived using Eq. (5).

$$\alpha(\omega) = \sqrt{2}\left[\sqrt{\varepsilon_1^2(\omega) + \varepsilon_2^2(\omega)} - \varepsilon_1(\omega)\right]^{1/2} \quad (5)$$

The calculated absorption spectra of the **A7** and **ZS** monolayers are illustrated in Fig. 4. The other optical properties along with the corresponding equations are presented in Figs. S3 and S4 in the Supporting Information. We have performed the calculation of the absorption spectra in three directions of the polarized incident light. Due to the symmetry constraints, the directions [100] and [010] are identical in the case of the **A7** sheet.

As one can see in Fig. 4, the positions of absorption peaks are in accord with the band structure plot (Fig. 2). It is interesting that the low-energy absorption (near 5 eV) corresponds to the [100] direction in both the **A7** and **ZS** monolayers, while for the light polarized along the perpendicular direction [001], the optical absorption is inactive around the band gap up to ca. 9 eV (the **A7** sheet) and ca. 6 eV (the **ZS** sheet).

The first absorption band in the spectrum of the **A7** monolayer is at about 5 eV (Fig. 4). As one can see in the band structure plot (Fig. 2), the VBM-CBM indirect transition is optically inactive. It is originated from electronic transitions from valence band to the isolated low energy block in the conduction band. For the **ZS** monolayer, two separated absorption peaks occur at ca. 1.5 and 3 eV (Fig. 4). The first absorption band corresponds to the direct VBM-CBM electron transition, while the second peak is a superposition of the two close-lying transitions from the VBM to the CBM + 1 and CBM + 2 at around the Γ-point (Fig. 2). Summing up, since the studied nitrogen monolayers, obviously, must be grafted on a substrate, their ultraviolet (UV) spectral detection should likely be done along the [001] direction of the polarized incident light. Therefore, the studied polynitrogen sheets are expected to be opaque to the UV irradiation only above ca. 9 and 6 eV for the **A7** and **ZS** monolayer, respectively.

In order to elucidate more information about the studied polynitrogen sheets, we have calculated the nuclear magnetic resonance (NMR) properties. The axes orientation and atomic labeling for the non-equivalent atoms are illustrated in Fig. 5, and the calculated data are listed in Table 2. The calculations are based on

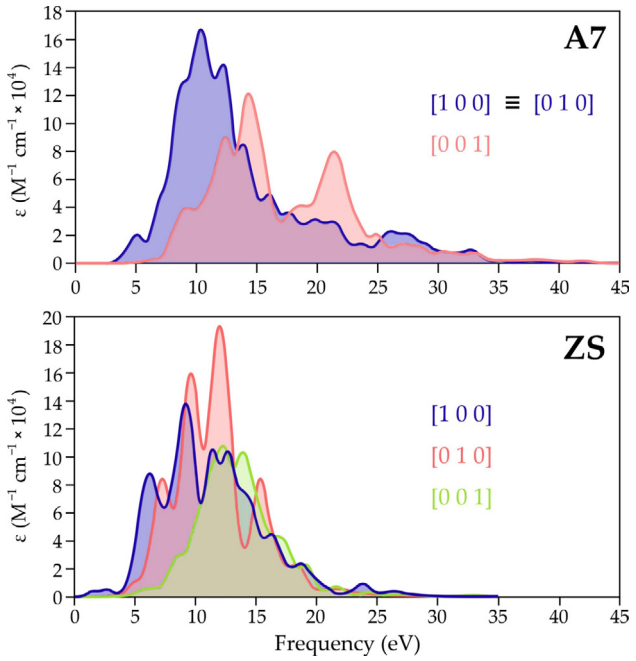

Fig. 4. The calculated absorption spectra of the studied polynitrogen sheets for different polarization vectors.

the estimation of the diagonal elements of magnetic shielding tensor (σ_{ij}). Thus, the isotropic chemical shielding (ppm) and the parameters of anisotropy and asymmetry have been calculated. For comparison, we have computed the same values for molecular nitrogen. As one can see in Table 2, the σ_{iso} values for the studied polynitrogen sheets are shifted towards a stronger field. This is attributed with a denser electron arrangement of the nitrogen nuclei compared to the N_2 molecule. The negative values of the anisotropy parameter (Δ) in the **ZS** sheet indicate the strong negative σ_{zz} components of magnetic shielding tensor.

Along with the NMR parameters, we have calculated the electric field gradient derived parameters, such as the quadrupolar coupling constants (C_Q) and the quadrupolar asymmetry parameter (η_Q) (Table 2). The C_Q constants have negative values in all the cases, including molecular nitrogen (Table 2). This indicates an axial elongated electronic charge distribution.

3.4. Mechanical and thermodynamic properties

The symmetry constraints require only five independent elastic constants in the case of the **A7** sheet ($P3m1$ wallpaper group) and nine constants for the **ZS** monolayer ($P2mm$ wallpaper group). According to the Born-Huang criteria, one can express four necessary and sufficient conditions for elastic stability in the hexagonal lattice case [57]:

$$\begin{cases} C_{11} > |C_{12}|;\ 2C_{13}^2 < C_{33}(C_{11} + C_{12}) \\ C_{44} > 0;\ C_{66} > 0 \end{cases} \quad (6)$$

For the orthorhombic lattice, the following criteria should be satisfied [57]:

$$\begin{cases} C_{11} > 0;\ C_{11}C_{22} > C_{12}^2 \\ C_{11}C_{22}C_{33} + 2C_{12}C_{13}C_{23} - C_{11}C_{23}^2 - C_{22}C_{13}^2 - C_{33}C_{12}^2 > 0 \\ C_{44} > 0;\ C_{55} > 0;\ C_{66} > 0 \end{cases} \quad (7)$$

The calculated elastic constants C_{ij} (N m^{-1}) for the **A7** sheet are the following: $C_{11} = 156.0$, $C_{12} = 14.7$, $C_{13} = -3.4$, $C_{33} = 1.5$ and $C_{44} = 4.6$. The **ZS** monolayer has the following elastic constants: $C_{11} = 117.0$, $C_{12} = 21.5$, $C_{13} = 0.9$, $C_{22} = 122.9$, $C_{23} = 1.5$, $C_{33} = 3.0$, $C_{44} = 3.5$, $C_{55} = 0.5$ and $C_{66} = 42.6$. The aforementioned values of elastic constants well satisfy the criteria (6) and (7). This reveals a robust mechanical stability of the **A7** and **ZS** sheets against stress around the equilibrium positions. All the calculated elastic constants (stiffness and compliance) are listed in Tables S1 and S2 in the Supporting Information.

Additionally, we have calculated the Young moduli and Poisson ratios along an arbitrary direction θ, which relates to the positive x direction in the sheet. Thus, the two polar diagrams can be obtained using the following equations [58]:

$$E(\theta) = \frac{\Delta}{C_{11}\sin^4\theta + C_{22}\cos^4\theta + \left(\frac{\Delta}{C_{44}} - 2C_{12}\right)\cos^2\theta\sin^2\theta} \quad (8)$$

$$\nu(\theta) = -\frac{\left(C_{11} + C_{22} - \frac{\Delta}{C_{44}}\right)\cos^2\theta\sin^2\theta - C_{12}(\cos^4\theta + \sin^4\theta)}{C_{11}\sin^4\theta + C_{22}\cos^4\theta + \left(\frac{\Delta}{C_{44}} - 2C_{12}\right)\cos^2\theta\sin^2\theta} \quad (9)$$

Herein, $\Delta = C_{11}C_{22} - C_{12}^2$. The plots of the obtained polar diagrams are illustrated in Fig. 6. Due to the symmetry restrictions, the polar diagrams for the **A7** monolayers demonstrate a perfect circle shape. Meanwhile, a strong anisotropy of $E(\theta)$ is observed in the case of the **ZS** sheet. However, the anisotropy of $\nu(\theta)$ is much less pronounced (Fig. 6). The largest Young modulus occurs in the x and y directions, while the smallest values characterize the angular bisectors of these directions (Fig. 6).

The corresponding Young moduli and Poisson ratios are listed in Table 3. As one can see in Table 3, the Young moduli of the **A7** monolayer are equal to 154 N m^{-1} that is much lower than that of graphene (345 N m^{-1}), but higher than that of recently calculated 2D porous tetraoxa [8] circulene (120 N m^{-1}) [59,60]. The latter value is close to the **ZS** sheet (Table 3).

Furthermore, we have calculated thermodynamic properties for the studied monolayers. These include zero-point vibrational energy (ZPE), enthalpy (H), Gibbs free energy (G), entropy (TS), heat capacity at constant volume (C_V) and the Debye temperature (θ_D) (Table 4). The latter is one of the fundamental constants of a solid and relates to the solid sound velocity and atomic vibration frequency; θ_D can be expressed in terms of average sound velocity:

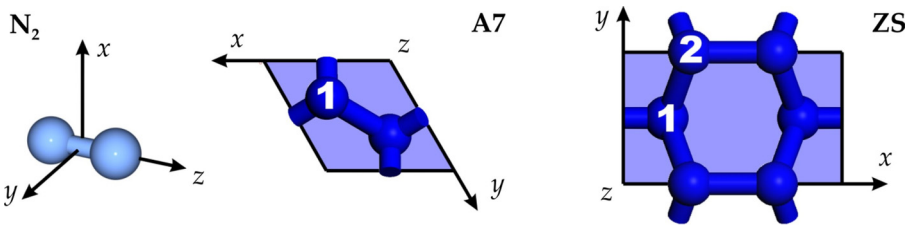

Fig. 5. The axes orientation and atom labeling in the **A7**, **ZS** nitrogen monolayers, and the N_2 molecule.

Table 2
Chemical shielding and electric field gradient (EFG) tensors at the symmetry unique atoms in the **A7** and **ZS** polynitrogen sheets for the ^{14}N isotope.

Atom	Shielding tensor			EFG tensor	
	σ_{iso} (ppm)	Δ (ppm)	η	C_Q (MHz)	η_Q
N1(**A7**)	−62.51	79.85	0.00	−5.217	0.00
N1(**ZS**)	−64.51	−60.33	0.84	−5.848	0.15
N2(**ZS**)	−64.36	−60.06	0.84	−5.851	0.15
N_2	−91.33	645.90	0.00	−5.599	0.00

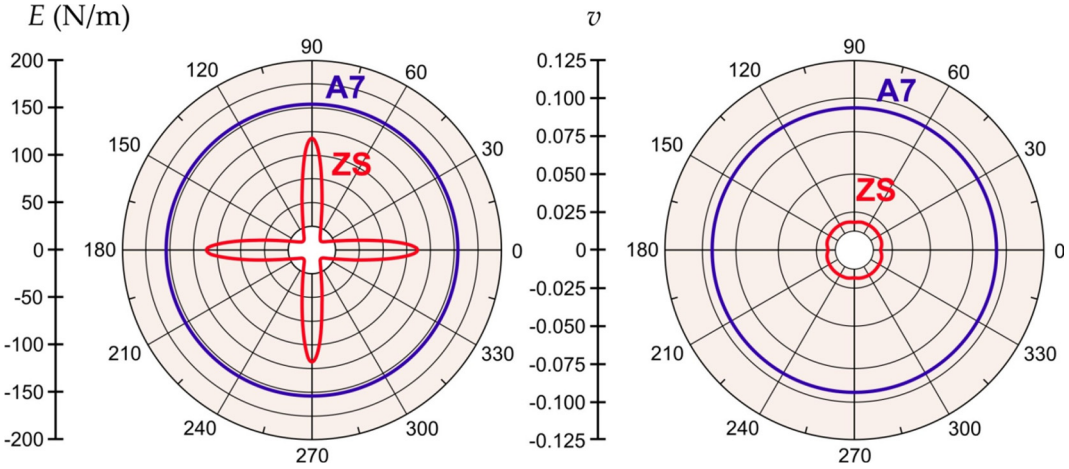

Fig. 6. Polar diagrams for the $E(\theta)$ (*left*) and $\nu(\theta)$ (*right*) of the **A7** (blue lines) and **ZS** (red lines) polynitrogen sheets. (For interpretation of the references to color in this figure legend, the reader is referred to the web version of this article.)

Table 3
Young Modulus (E, GPa) and Poisson Ratios (ν) for the polynitrogen sheets studied.

Axis	E (N m^{-1})	Poisson ratios (ν)			
A7					
x	153.581	E_{xy}	0.0752	E_{xz}	1.5359
y	153.581	E_{yx}	0.0752	E_{yz}	1.5359
z	1.184	E_{zx}	0.0118	E_{zy}	0.0118
ZS					
x	113.096	E_{xy}	0.1721	E_{xz}	0.2097
y	118.309	E_{yx}	0.1801	E_{yz}	0.4532
z	2.985	E_{zx}	0.0055	E_{zy}	0.0114

Table 4
The calculated thermodynamic properties (at 298 K) for the **A7** and **ZS** polynitrogen sheets studied.

Sheet	ZPE[a]	H[b]	G[b]	TS[b]	C_V[c]	Θ_D[d]
A7	0.2506	2.6637	−1.4038	4.0675	5.4707	1358
ZS	0.4061	6.5950	−2.9743	9.5694	13.6117	1147

[a] Zero point energy in eV.
[b] The values in kJ mol^{-1}.
[c] The values in cal cell^{-1} K^{-1}.
[d] The values correspond to the high temperature limit (K).

$$\theta_D = \frac{h}{k_B}\left[\frac{3n}{4\pi}\left(\frac{N_A\rho}{M}\right)\right]^{1/3} v_m \quad (10)$$

Herein, h is the Planck constant, k_B the Boltzmann constant, n the number of atoms per unit cell, N the Avogadro number, ρ the crystal density, M the molecular weight, and v_m is the average sound velocity.

The corresponding plots of the temperature dependence of the thermodynamic properties are illustrated in Fig. S5 in the Supporting Information. As one can see in Fig. S5, the estimated value of the Debye temperature for the **A7** sheet is 878.52 K at 48.91 K. Meanwhile, in the case of the **ZS** monolayer the Debye temperature corresponds to 1229.46 K at 30.40 K. We should stress that the high temperature limit occurs at a lower temperature being equal to 1147 K (Table 4).

4. Conclusions

In summary, we have studied structure, spectra, stability and mechanical properties of two possible types of 2D materials constructed from single-bonded nitrogen atoms forming the honey-

comb (**A7**) and zigzag sheet (**ZS**) monolayers. The calculated band structure and partial density of states illustrate the semiconducting properties of the **ZS** polymer while the **A7** structure can be characterized as an insulator. The value of band gap in the **ZS** sheet characterizes this structure as a desirable 2D material for the next-generation optoelectronics. Thus, our calculation provides a new outlook on various properties of single-bonded nitrogen 2D monolayers which can present high-energy density properties being, at the same time, potential candidates for molecular electronics and photonics.

We should stress that in a recent paper of Yao et al. [4], the DFT calculations of 2D materials with the honeycomb (**A7**) lattice based on octet stability for the whole family of pnictogens (N, P, As, Sb, Bi) are also presented. But the characterization of the materials is restricted by only a structural analysis and electronic properties calculations. Our structural results are very close to these previously obtained (the N—N bond length is 1.50 Å [4] against our 1.526 Å, $a = 2.3$ Å [4] against our 2.325 Å value). Meanwhile, in the present paper we report on a comprehensive theoretical study of 2D polynitrogen materials including the complete structural and spectral representation, thermodynamic and mechanical study and provide a guide for further study of hybrid nitrogen materials [6]. Additionally, Yao et al. [4] have also calculated spin-orbit coupling (SOC) effects for orbitals involved in the structures near Fermi level and found large SOC for all pnictogens except nitrogen. Thus, our DFT approximation without SOC is quite reasonable [61].

Acknowledgment

This work was supported by the Ministry of Education and Science of Ukraine, Research Fund (Grant No. 0113U001694). The computations were performed on resources provided by the Swedish National Infrastructure for Computing (SNIC) at the Parallel Computer Center (PDC) through the project "Multiphysics Modeling of Molecular Materials", SNIC 020/11-23. We thank Professor Hans Ågren (KTH, Stockholm) for the PDC supercomputer use.

Appendix A. Supplementary material

Supplementary data associated with this article can be found, in the online version, at http://dx.doi.org/10.1016/j.commatsci.2017.03.007.

References

[1] K.S. Novoselov, A.K. Geim, S.V. Morozov, D. Jiang, Y. Zhang, S.V. Dubonos, I.V. Grigorieva, A.A. Firsov, Electric field effect in atomically thin carbon films, Science 306 (2004) 666–669.
[2] R. Mas-Ballesté, C. Gómez-Navarro, J. Gómez-Herrero, F. Zamora, 2D materials: to graphene and beyond, Nanoscale 3 (2011) 20–30.
[3] Y. Harada, M. Yamamoto, T. Baba, T. Kita, Epitaxial two-dimensional nitrogen atomic sheet in GaAs, Appl. Phys. Lett. 104 (2014) 041907.
[4] J. Lee, W.-C. Tian, W.-L. Wang, D.-X. Yao, Two-dimensional pnictogen honeycomb lattice: structure, on-site spin-orbit coupling and spin polarization, Sci. Rep. 5 (2015) 11512.
[5] A. Hu, F. Zhang, T. Woo, Metastable polymeric nitrogen nanotube from a zigzag sheet phase and first-principles calculations, Phys. Rev. B 82 (2010) 125410.
[6] N.N. Karaush, S.V. Bondarchuk, G.V. Baryshnikov, V.A. Minaeva, W.-H. Sun, B.F. Minaev, Computational study of the structure, UV-vis absorption spectra and conductivity of biphenylene-based polymers and their boron nitride analogues, RSC Adv. 6 (2016) 49505–49516.
[7] M. Zhang, G. Gao, A. Kutana, Y. Wang, X. Zou, J.S. Tse, B.I. Yakobson, H. Li, H. Liu, Y. Ma, Two-dimensional boron-nitrogen-carbon monolayers with tunable direct band gaps, Nanoscale 7 (2015) 12023–12029.
[8] J. Mahmood, E.K. Lee, M. Jung, D. Shin, I.-Y. Jeon, S.-M. Jung, H.-J. Choi, J.-M. Seo, S.-Y. Bae, S.-D. Sohn, N. Park, J.H. Oh, H.-J. Shin, J.-B. Baek, Nitrogenated holey two-dimensional structures, Nat. Commun. 6 (2015) 6486.
[9] S.S. Yu, W.T. Zheng, Q. Jiang, Electronic properties of nitrogen-atom-adsorbed graphene nanoribbons with armchair edges, IEEE Trans. Nanotechnol. 9 (2010) 243–247.
[10] J.R. Owens, E. Cruz-Silva, V. Meunier, Electronic structure and transport properties of N_2^{AA}-doped armchair and zigzag graphene nanoribbons, Nanotechnology 24 (2013) 235701.
[11] Z. Shang-Qian, L. Yan, L. Wen-Gang, L. Wen-Jie, W. En-Ge, Modulating magnetism of nitrogen-doped zigzag graphene nanoribbons, Chin. Phys. B 23 (2014) 067305.
[12] S.S. Yu, W.T. Zheng, Q.B. Wen, Q. Jiang, First principle calculations of the electronic properties of nitrogen-doped carbon nanoribbons with zigzag edges, Carbon 46 (2008) 537–543.
[13] S. Kumar Jain, P. Srivastava, Effect of nitrogen impurity on electronic properties of boron nanotubes, Adv. Cond. Matter Phys. 2014 (2014) 706218.
[14] R. Gong, F. Du, Z. Xia, M. Durstock, L. Dai, Nitrogen-doped carbon nanotube arrays with high electrocatalytic activity for oxygen reduction, Science 323 (2009) 760–764.
[15] Z. Wu, E.M. Benchafia, Z. Iqbal, X. Wang, N_8^- Polynitrogen stabilized on multi-wall carbon nanotubes for oxygen-reduction reactions at ambient conditions, Angew. Chem. 126 (2014) 1–6.
[16] S.-S. Li, H.-P. Cong, P. Wanga, S.-H. Yu, Flexible nitrogen-doped graphene/carbon nanotube/Co_3O_4 paper and its oxygen reduction activity, Nanoscale 6 (2014) 7534–7541.
[17] L.S. Panchakarla, A. Govindaraj, C.N.R. Rao, Boron- and nitrogen-doped carbon nanotubes and graphene, Inorg. Chim. Acta 363 (2010) 4163–4174.
[18] T.M. Klapötke, New nitrogen-rich high explosives, in: T.M. Klapötke (Ed.), High Energy Density Materials, vol. 125, Springer-Verlag GmbH, Berlin, 2007, pp. 85–121.
[19] M.N. Glukhovtsev, H. Jiao, P.v.R. Schleyer, Besides N_2, what is the most stable molecule composed only of nitrogen atoms?, Inorg Chem. 35 (1996) 7124–7133.
[20] S. Ajith Perera, R.J. Bartlett, Coupled-cluster calculations of raman intensities and their application to N_4 and N_5^-, Chem. Phys. Lett. 314 (1999) 381–387.
[21] A. Vij, J.G. Pavlovich, W.W. Wilson, V. Vij, K.O. Christe, Experimental detection of the pentaazacyclopentadienide (pentazolate) anion, cyclo-N_5^-, Angew. Chem. Int. Ed. 41 (2002) 3051–3054.
[22] A. Vij, W.W. Wilson, V. Vij, F.S. Tham, J.A. Sheehy, K.O. Christe, Polynitrogen chemistry. Synthesis, characterization, and crystal structure of surprisingly stable fluoroantimonate salts of N_5^+, J. Am. Chem. Soc. 123 (2001) 6308–6313.
[23] B.A. Steele, E. Stavrou, J.C. Crowhurst, J.M. Zaug, V.B. Prakapenka, I.I. Oleynik, High-pressure synthesis of a pentazolate salt, Chem. Mater. 29 (2017) 735–741.
[24] K.O. Christe, W.W. Wilson, J.A. Sheehy, J.A. Boatz, N_5^+: a novel homoleptic polynitrogen ion as a high energy density material, Angew. Chem. Int. Ed. 38 (1999) 2004–2009.
[25] H. Huber, Is hexazine stable?, Angew Chem. Int. Ed. 21 (1982) 64–65.
[26] P. Saxe, H.F. Schaefer III, Cyclic D_{6h} hexaazabenzene—a relative minimum on the N_6 Potential Energy Hypersurface?, J Am. Chem. Soc. 105 (1983) 1760–1764.
[27] T.M. Klapötke, Ab initio calculations of the open-chain N_6 diazide molecule, J. Mol. Struct. (THEOCHEM) 499 (2000) 99–104.
[28] M.N. Glukhovtsev, P.v.R. Schleyer, Structures, bonding and energies of N_6 isomers, Chem. Phys. Lett. 198 (1992) 547–554.
[29] M. Tobita, R.J. Bartlett, Structure and stability of N_6 isomers and their spectroscopic characteristics, J. Phys. Chem. A 105 (2001) 4107–4113.
[30] T.M. Klapötke, R.D. Harcourt, The interconversion of N_{12} to N_8 and two equivalents of N_2, J. Mol. Struct. (THEOCHEM) 541 (2001) 237–242.
[31] M.R. Manaa, Toward new energy-rich molecular systems: from N_{10} to N_{60}, Chem. Phys. Lett. 331 (2000) 262–268.
[32] L.J. Wang, M.Z. Zgierski, Super-high energy-rich nitrogen cluster N_{60}, Chem. Phys. Lett. 376 (2003) 698–703.
[33] A.K. McMahan, R. LeSar, Pressure dissociation of solid nitrogen under 1 Mbar, Phys. Rev. Lett. 54 (1985) 1929–1932.
[34] C. Mailhiot, L.H. Yang, A.K. McMahan, Polymeric nitrogen, Phys. Rev. B 46 (1992) 14419–14435.
[35] M.I. Eremets, A.G. Gavriliuk, I.A. Trojan, D.A. Dzivenko, R. Boehler, Single-bonded cubic form of nitrogen, Nat. Materials 3 (2004) 558–563.
[36] M.I. Eremets, M.Yu. Popov, I.A. Trojan, V.N. Denisov, R. Boehler, R.J. Hemley, Polymerization of nitrogen in sodium azide, J. Chem. Phys. 120 (2004) 10618–10623.
[37] M.I. Eremets, A.G. Gavriliuk, N.R. Serebryanaya, I.A. Trojan, D.A. Dzivenko, R. Boehler, H.K. Mao, R.J. Hemley, Structural transformation of molecular nitrogen to a single-bonded atomic state at high pressures, J. Chem. Phys. 121 (2004) 11296–11300.
[38] T.M. Klapötke, P. Mayer, A. Schulz, J.J. Weigand, 1,5-Diamino-4-methyltetrazolium dinitramide, J. Am. Chem. Soc. 127 (2005) 2032–2033.
[39] U.N. Patil, N.R. Dhumal, S.P. Gejji, Theoretical studies on the molecular electron densities and electrostatic potentials in azacubanes, Theor. Chem. Acc. 112 (2004) 27–32.
[40] J.P. Agrawal, High Energy Materials: Propellants, Explosives and Pyrotechnics, Wiley-VCH, Weinheim, 2010, pp. 141–144.
[41] Y.-C. Li, C. Qi, S.-H. Li, H.-J. Zhang, C.-H. Sun, Y.-Z. Yu, S.-P. Pang, 1,1-Azobis-1,2,3-triazole: a high-nitrogen compound with stable N8 structure and photochromism, J. Am. Chem. Soc. 132 (2010) 12172–12173.
[42] V.E. Zarko, Searching for ways to create energetic materials based on polynitrogen compounds (review), Combust. Expl. Shock Waves 46 (2010) 121–131.
[43] M.W. Schmidt, M.S. Gordon, J.A. Boatz, Triazolium-based energetic ionic liquids, J. Phys. Chem. A 109 (2005) 7285–7295.

[44] R. Wang, H. Gao, Ch. Ye, B. Twamley, J.M. Shreeve, Heterocyclic-based nitrodicyanomethanide and dinitrocyanomethanide salts: a family of new energetic ionic liquids, Inorg. Chem. 46 (2007) 932–938.
[45] J. Geith, T.M. Klapötke, J. Weigand, Calculation of the detonation velocities and detonation pressures of dinitrobiuret (DNB) and diaminotetrazolium nitrate (HDAT-NO_3), Prop. Explos. Pyrotech. 29 (2004) 3–8.
[46] S.V. Bondarchuk, B.F. Minaev, Super high-energy density single-bonded trigonal nitrogen allotrope—a chemical twin of the cubic gauche form of nitrogen, Phys. Chem. Chem. Phys. 19 (2017) 6698–6706.
[47] S.J. Clark, M.D. Segall, C.J. Pickard, P.J. Hasnip, M.J. Probert, K. Refson, M.C. Payne, First principles methods using CASTEP, Z. Kristallogr. 220 (2005) 567–570.
[48] Materials Studio 7.0, Accelrys Inc., San Diego, CA, 2013.
[49] J.P. Perdew, K. Burke, M. Ernzerhof, Generalized gradient approximation made simple, Phys. Rev. Lett. 77 (1996) 3865–3868.
[50] A. Tkatchenko, M. Scheffler, Accurate molecular van der Waals interactions from ground-state electron density and free-atom reference data, Phys. Rev. Lett. 102 (2009) 3005–3008.
[51] S.V. Bondarchuk, B.F. Minaev, Thermally accessible triplet state of π-nucleophiles does exist. Evidence from first principles study of ethylene interaction with copper species, RSC Adv. 5 (2015) 11558–11569.
[52] D. Hanlon, C. Backes, E. Doherty, C.S. Cucinotta, N.C. Berner, C. Boland, K. Lee, A. Harvey, P. Lynch, Z. Gholamvand, S. Zhang, K. Wang, G. Moynihan, A. Pokle, Q. M. Ramasse, N. McEvoy, W.J. Blau, J. Wang, G. Abellan, F. Hauke, A. Hirsch, S. Sanvito, D.D. O'Regan, G.S. Duesberg, V. Nicolosi, J.N. Coleman, Liquid exfoliation of solvent-stabilized few-layer black phosphorus for applications beyond electronics, Nat. Commun. 6 (2015) 8563.
[53] Q.H. Wang, K. Kalantar-Zadeh, A. Kis, J.N. Coleman, M.S. Strano, Electronics and optoelectronics of two-dimensional transition metal dichalcogenides, Nat. Nanotech. 7 (2012) 699.
[54] Z. Zhu, D. Tománek, Semiconducting layered blue phosphorus: a computational study, Phys. Rev. Lett. 112 (2014) 176802.
[55] J.A. Alarco, A. Chou, P.C. Talbota, I.D.R. Mackinnon, Phonon modes of MgB_2: super-lattice structures and spectral response, Phys. Chem. Chem. Phys. 16 (2014) 24443–24456.
[56] M. Sheik-Bahae, Nonlinear optics basics. Kramers-Kronig relations in nonlinear optics, in: R.D. Guenther (Ed.), Encyclopedia of Modern Optics, Academic Press, Amsterdam, 2005, pp. 234–239.
[57] F. Mouhat, F.-X. Coudert, Necessary and sufficient elastic stability conditions in various crystal systems, Phys. Rev. B 90 (2014) 224104.
[58] E. Cadelano, P.L. Palla, S. Giordano, L. Colombo, Elastic properties of hydrogenated graphene, Phys. Rev. B 82 (2010) 235414.
[59] J. Yu, Q. Sun, Y. Kawazoe, P. Jena, Stability and properties of 2D porous nanosheets based on tetraoxa[8]circulene analogues, Nanoscale 6 (2014) 14962–14970.
[60] G.V. Baryshnikov, B.F. Minaev, N.V. Karaush, V.A. Minaeva, Design of nanoscaled materials based on tetraoxa[8]circulene, Phys. Chem. Chem. Phys. 16 (2014) 6555–6559.
[61] H. Ågren, O. Vahtras, B. Minaev, Response theory and calculations of spin-orbit coupling phenomena in molecules, Adv. Quant. Chem. 27 (1996) 71–162.